Journal of Alloys and Compounds 509 (2011) 4547–4552

Contents lists available at ScienceDirect

Journal of Alloys and Compounds

journal homepage: www.elsevier.com/locate/jallcom

Fast fabrication of Co_3O_4 and $CuO/BiVO_4$ composite photocatalysts with high crystallinity and enhanced photocatalytic activity *via* ultrasound irradiation

Changlin Yu [a,*], Kai Yang [a], Jimmy C. Yu [b], Fangfang Cao [a], Xin Li [a], Xiaochun Zhou [a]

[a] School of Materials and Chemical Engineering, Jiangxi University of Science and Technology, 86 Hongqi Road, Ganzhou 341000, Jiangxi, China
[b] Department of Chemistry, The Center of Novel Functional Molecules, and Environmental Science Programme, The Chinese University of Hong Kong, Shatin, New Territories, Hong Kong, China

ARTICLE INFO

Article history:
Received 3 October 2010
Received in revised form 11 January 2011
Accepted 15 January 2011
Available online 22 January 2011

Keywords:
$BiVO_4$
Ultrasonic irradiation
p–n Heterojunction
Crystallinity
Photocatalysis

ABSTRACT

A facile and efficient approach for the fabrication of Co_3O_4 and $CuO/BiVO_4$ composite photocatalysts was developed by intense ultrasound irradiation at room temperature. The as-synthesized samples were characterized by X-ray diffraction (XRD), X-ray photoelectron spectroscopy (XPS), scanning electron microscopy (SEM), photoluminescence (PL) spectroscopy, UV–vis diffuse reflectance spectra (UV–vis DRS), and Brunauer–Emmett–Teller (BET) surface areas. The photocatalytic activity of the composite catalysts was evaluated by photocatalytic degradation of acid orange II under visible light ($\lambda > 420$ nm) irradiation. Results showed that under intense ultrasonic irradiation, the precursors of copper acetate and cobaltous acetate could transform into CuO and Co_3O_4, respectively and the amorphous $BiVO_4$ can easily crystallize to highly crystalline $BiVO_4$. The composite photocatalysts exhibited much higher photocatalytic activity than that of pure $BiVO_4$. The enhanced photocatalytic performance could be attributed to the high crystallinity of $BiVO_4$ and the formed p–n heterojunction of $Co_3O_4/BiVO_4$ or $CuO/BiVO_4$. These two factors can effectively suppress the recombination of photogenerated hole–electron pairs.

1. Introduction

Nowadays, photocatalysis based on the utilization of solar energy has attracted much attention due to its promising applications in environmental treatments [1–9]. Among the photocatalysts, TiO_2 has received the most attention as a photocatalytic material because of its chemical and physical durability, high activity, nontoxicity, and low cost [10,11]. However, a major drawback of TiO_2 is its large band gap of 3.2 eV which corresponds to excitation wavelengths below 390 nm. So wavelengths below 400 nm are necessary for excitation and only the small UV fraction of solar light, about 2–3%, can be utilized, which greatly limits its effective application of solar energy. Therefore TiO_2 is not effective for solar-driven applications. It is necessary to develop the visible light driven photocatalysts with high efficiency.

Recently, a great number of novel semiconductor photocatalysts with visible light response have been developed, such as BiOI [9,12], $Ag\text{-}AgI/Al_2O_3$ [8], $g\text{-}C_3N_4$ [13], Cd_2SnO_4 [14], $LaNiO_3$ [15], $CdBiO_2Cl$ [16], etc. They all exhibit certain absorption ability in the visible light range. These findings provide new insights for the design of non-titania based visible light driven semiconductor photocatalysts. Bismuth vanadate ($BiVO_4$) is one of the non-titania based visible light driven semiconductor photocatalysts [17–19]. It has been found that the photocatalytic activity of $BiVO_4$ is determined by its crystal phase. $BiVO_4$ with a monoclinic scheelite structure can show photocatalytic properties and is commonly used as photocatalyst in water splitting and oxidative decomposition of organic contaminants under visible light irradiation [20,21]. However, the activity of pure $BiVO_4$ is not high enough for the requirements of large-scale application. It was reported that the addition of transition metal oxides to $BiVO_4$ could give an obvious increase in photocatalytic activity [22]. Moreover, the photocatalytic performance of $BiVO_4$ also strongly depends on its preparation method.

Sonochemical processing has been proven to be a unique and effective method to synthesize novel materials with unusual properties [1,23–25]. The effects of acoustic cavitation from the ultrasound irradiation in a liquid could produce the extreme conditions, such as the extremely high temperatures (~5000 °C), pressures (>20 MPa), and cooling rates (>$10^{9\circ}$ s^{-1}). These extreme conditions have been exploited to accelerate the crystallization of metal oxides under low temperatures [26,23,27,28]. Our recent research has shown that under ultrasound irradiation an efficient process of fluorine doping and crystallization could take place over the amorphous TiO_2 sol particles [1].

In this study, we described a facile and efficient approach for fabrication of Co_3O_4 and $CuO/BiVO_4$ composite photocatalysts *via* ultrasound irradiation at room temperature. The obtained photocatalysts have high crystallinity and enhanced photocatalytic

* Corresponding author. Tel.: +86 797 8312204; fax: +86 797 8312204.
E-mail address: yuchanglinjx@163.com (C. Yu).

0925-8388/$ – see front matter © 2011 Elsevier B.V. All rights reserved.
doi:10.1016/j.jallcom.2011.01.100

activity. To the best of our knowledge, it is the first time to report the preparation of metal oxide composite photocatalysts by a sonochemical approach.

2. Experimental

2.1. Synthesis

4.0 g nonionic surfactant of P123 (triblock copolymer templates), 50 mL deionized (DI) water and 10 mL alcohol, 6.5 mL 69%HNO_3, 4.850 g $Bi(NO_3)\cdot 5H_2O$ were mixed, obtained solution A; 1.170 g NH_4VO_3, 40 mL DI water, 1.600 g NaOH were mixed, obtained solution B. Solution B was added dropwise to solution A under stirring. The pH value of the mixture was adjusted to 7 by 4 mol/L NaOH. Then the mixture was exposed to high-intensity ultrasound irradiation under ambient air. At the same time, appropriate amount of copper acetate or cobaltous acetate was introduced to the mixture. Ultrasound irradiation was accomplished with a high-intensity ultrasonic probe (XinzhiCo., Ningbo, China, JY92-2D, 1.2 cm diameter; Ti-horn, 20 kHz, 60 W/cm^2) immersed directly in the reaction solution, and the total reaction time lasted for 180 min. The precipitate was centrifuged, washed with DI water and absolute ethanol in sequence, and finally dried in air for 12 h at 120 °C. The final content of Co and Cu in $BiVO_4$ was determined by X-ray fluorescence analysis (Magix 601), which were marked as Co(1%)/$BiVO_4$, Co(3%)/$BiVO_4$, Cu(1%)/$BiVO_4$ and Cu(3%)/$BiVO_4$ indicating the wt.% amount of Co and Cu in the catalyst.

2.2. Characterization

Powder X-ray diffraction data were recorded at a scanning rate of 0.01° s^{-1} using a Bruker D8-advance X-ray diffractometer at 40 kV and 40 mA for monochromatized Cu Kα (λ = 1.5418 Å) radiation. The surface composition was determined by X-ray photoelectron spectroscopy (XPS) using a PHI Quantum 2000 XPS system with a monochromatic Al Ka source and a charge neutralizer. All the binding energies were referenced to the C 1s peak at 284.8 eV of the surface adventitious carbon. Scanning electron microscopy (SEM) measurements were carried out on a LEO 1450VP scanning electron microscope to investigate the morphology and surface roughness of samples. The products were conductively coated with gold by sputtering for 30 s to minimize charging effects under SEM imaging conditions. To investigate the recombination and lifespan of photogenerated electrons/holes in the photocatalysts, the photoluminescence (PL) emission spectra of the samples were recorded. A 320 nm He–Cd laser was used as an excitation light source. The emission from the sample was measured by a spectrometer (Spex 500 M, USA) equipped with a photon counter (SR400, USA). UV–vis diffuse reflectance spectra (UV–vis DRS) were achieved using a UV–vis spectrophotometer (Cary 100 scan spectrophotometers, Varian). Absorption spectra were referenced to $BaSO_4$. The Brunauer–Emmett–Teller (BET) surface areas of the sample was obtained from N_2 adsorption/desorption isotherms determined at liquid nitrogen temperature on an automatic analyzer (ASAP 2010). The samples were outgassed for 2 h under vacuum at 180 °C prior to adsorption.

2.3. Photocatalytic activity test

The photocatalytic activities of the samples were determined by measuring the degradation of acid orange II in an aqueous solution under visible light irradiation. In activity test, a 300 W tungsten halogen lamp with a λ < 420 nm cutoff filter was used as visible light source. The photocatalyst (0.05 g) was suspended in 80 mL aqueous solution of acid orange II with the concentration of C_0 = 0.020 g/L. Prior to light illumination, the suspension was strongly magnetically stirred for 40 min in the dark for adsorption/desorption equilibrium. The suspension was vigorously stirred with the photoreactor during the process and the temperature of suspension was maintained at 22 °C by circulation of water through an external cooling coil. At given intervals of illumination, the sample of suspension was taken out and centrifuged. The clear upper layer solution was analyzed by a Milton Roy Spectronic 3000 Array spectrophotometer (New York, USA). The dye concentration was measured at λ = 484 nm, the maximum absorption wavelength for acid orange II.

3. Results and discussion

3.1. XRD analysis

The XRD patterns for the pure $BiVO_4$ and $BiVO_4$ composites are shown in Fig. 1. Clear characteristic peaks with 2θ at 18.8°, 28.6°, 30.5°, 35.2°, 39.7° and 53.1° are observed, which are indexed to the standard cards (JCPDS No.14-0688). These diffraction peaks indicate that all samples are monoclinic scheelite structure with high crystallinity. The calculated lattice constants of a = 5.17, b = 11.72, and c = 5.09 Å are in agreement with the reported values (a = 5.19, b = 11.70, and c = 5.09 Å, JCPDS No. 14-0688). This result demonstrates that pure monoclinic $BiVO_4$ with high crystallinity can be fast fabricated by powerful ultrasonic irradiation at room temperature. The extreme chemical conditions arising from acoustic cavitation could play the important role in the formation of $BiVO_4$ crystals. The transient high-temperature (~5000 °C) and high-pressure (>20 MPa) field produced during ultrasound irradiation could provide a favorable environment for the crystallization of amorphous $BiVO_4$. It has been reported that $BiVO_4$ has three main crystal phases: tetragonal zircon structure, monoclinic scheelite structure, and tetragonal scheelite structure [29]. The phase transition can take place at different temperatures or even by crushing the powder at room temperature. In our ultrasound irradiation conditions, the pure monoclinic scheelite was obtained. Among the three crystal phases, only the monoclinic scheelite structure $BiVO_4$ can exhibit good photocatalytic performance under visible light irradiation. Therefore, this ultrasound prepared $BiVO_4$ is suited for the photocatalytic test. The average crystallite sizes of $BiVO_4$ were determined by the Scherrer equation using the fwhm data of 1 2 1 crystalline plane. The calculation crystallite sizes for $BiVO_4$, Co(1%)/$BiVO_4$, Co(3%)/$BiVO_4$, Cu(1%)/$BiVO_4$ and Cu(3%)/$BiVO_4$ are 20.70, 22.27, 20.63, 19.31 and 20.69 nm, respectively. No diffraction peaks of Co or Cu species are observed over the composite samples, which is due to the small crystallite size or low concentration of Co or Cu species.

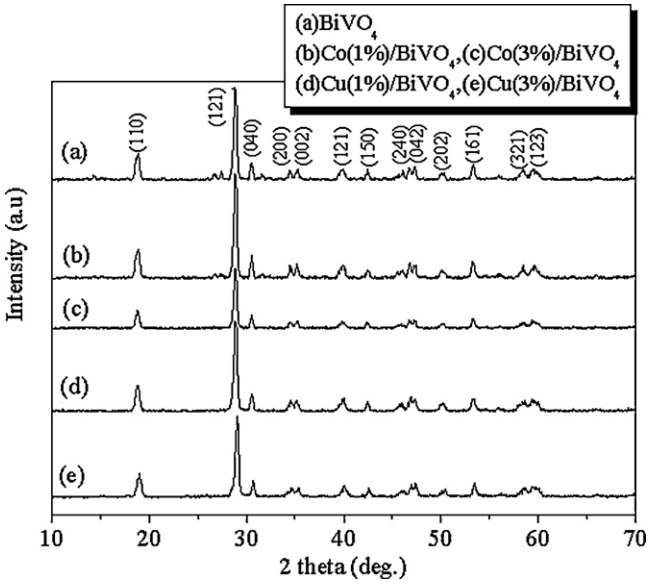

Fig. 1. X-ray diffraction patterns of the $BiVO_4$ and Co and Cu/$BiVO_4$ composite samples.

3.2. Microstructures analysis

The morphology of the synthesized samples was analyzed by SEM. Fig. 2 shows the three typical SEM images of the $BiVO_4$, Cu(1%)/$BiVO_4$ and Co(3%)/$BiVO_4$ photocatalysts. It is observed that all three samples are composed of a large quantity of well dispersed uniform particles. In addition, the BET surface area of the samples was determined by N_2 adsorption. The BET surface areas of $BiVO_4$, Co(1%)/$BiVO_4$, Co(3%)/$BiVO_4$, Cu(1%)/$BiVO_4$ and Cu(3%)/$BiVO_4$ were estimated to be 6.20, 7.04, 8.03, 8.78, and 8.03 m^2/g, respectively. The surface area values of these samples are much bigger than that in literature [30] in which the sample was prepared by common solution method. It is reasonable to infer that the high intensity ultrasound irradiation could benefit not only the crystallization of $BiVO_4$ but also the formation of small and well dispersed $BiVO_4$ crystals. The diminishing of the particles could cause an increase in the surface area of the sample.

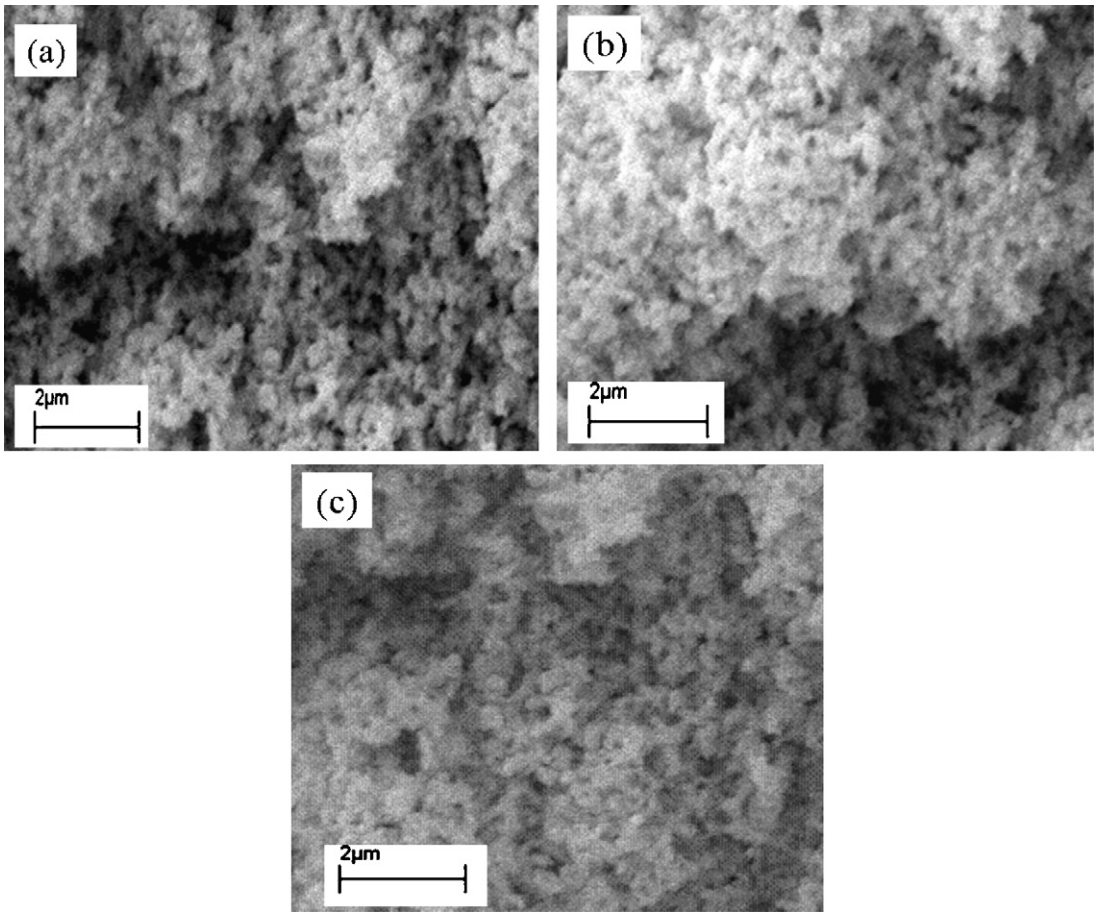

Fig. 2. The SEM images of the samples. (a) $BiVO_4$; (b) Cu(1%)/$BiVO_4$; (c) Co(3%)/$BiVO_4$.

3.3. XPS study

In order to investigate the chemical state of the elements in Co or Cu/$BiVO_4$ composites, especially to study the oxidation state of Cu and Co, XPS spectra of Cu(1%)/$BiVO_4$ and Co(3%)/$BiVO_4$ were obtained by scanning the O 1s, V 2p, Bi 4f, Cu 2p and Co 2p. The quantitative analysis of the results of XPS shows that the wt.% of Cu, Bi, V and O elements in Cu(1%)/$BiVO_4$ are 0.95, 63.70, 15.51, and 19.82%, respectively and Co, Bi, V and O elements in Co(3%)/$BiVO_4$ are 2.94, 61.92, 14.94, and 20.21%, respectively, which is almost consistent with the results of X-ray fluorescence analysis. The high resolution XPS spectra of Cu(1%)/$BiVO_4$ are displayed in Fig. 3(a)–(d). The asymmetric XPS of O 1s indicates that different oxygen species are present in the near surface region. They are the lattice oxygen (530.3 eV) in crystalline $BiVO_4$ or CoO_x (CuO) and the chemisorbed OH^- (531.6 eV) on the surface [30,31]. The V 2p orbital shows the peaks at 516.9 and 523.9 eV, as indicated in Fig. 3(b). Fig. 3(c) gives the high-resolution XPS spectrum of the Bi 4f. The Bi 4f spectrum can perfectly be deconvoluted into two peaks. The peaks with binding energy of 158.4 and 163.7 eV are for the Bi 4f7/2 and Bi 4f5/2 region in $BiVO_4$, respectively. The chemical state of Bi in the sample is found +3 valence. The high-resolution XPS spectra of the Cu 2p region are shown in Fig. 3(d). The characteristic peaks at 935.4 and 955.5 eV are ascribed to the Cu 2p3/2 and Cu 2p1/2, respectively, which is consistent with the results of Xu's report [30]. Therefore, it confirms that Cu exists as CuO in the Cu/$BiVO_4$ composite. The high-resolution XPS spectrum of Co/$BiVO_4$ sample reveals the Co 2p3/2 and Co 2p1/2 peaks at 779.6 and 797.0 eV, respectively, as shown in Fig. 3(e). These two peaks are close to those of Co_3O_4, whose corresponding peaks were reported at 780.8 and 796.8 eV [32].

3.4. UV–vis DRS analysis

The UV–vis DRS of the pure and $BiVO_4$ composite catalysts are shown in Fig. 4. All samples exhibit different absorptions in the visible light region. The absorption edge of pure $BiVO_4$ is determined to be 529 nm. The corresponding band-gap energy for the pure $BiVO_4$ catalyst is 2.34 eV which is determined with Tauc's law from the intercept of a straight line fitted through the rise of the function $[F(Ra)hm]^2$ plotted versus hm, where $F(Ra)$ is a Kubelka–Munk function and hm is the energy of the incident photon [33,34]. It is slightly smaller than the reported values [30]. The presence of Co_3O_4 results in an increase in the ability of visible light absorption, which should be attributed to the small band gap of Co_3O_4 which is a p-type semiconductor with direct transition at 1.45 and 2.07 eV [35], corresponding respectively to edges of $O^{2-} \rightarrow Co^{3+}$ excitation and $O^{2-} \rightarrow Co^{2+}$ charge transfer. The latter is the basic optical band gap energy for interband transitions [35,36]. Co_3O_4 has absorption in nearly all of the visible light range and induces an extension of the light absorption spectrum of the composite semiconductor even at low cobalt contents. As for the CuO/$BiVO_4$, no distinct shift in absorption edge appears compared with the pure $BiVO_4$. According to the report of literature [30], loading CuO over $BiVO_4$ could cause a red shift in light absorption edge. The observed weak red shift over CuO/$BiVO_4$ is caused by the charge-transfer transition between the metal ions and the $BiVO_4$ conduction or valance band [37].

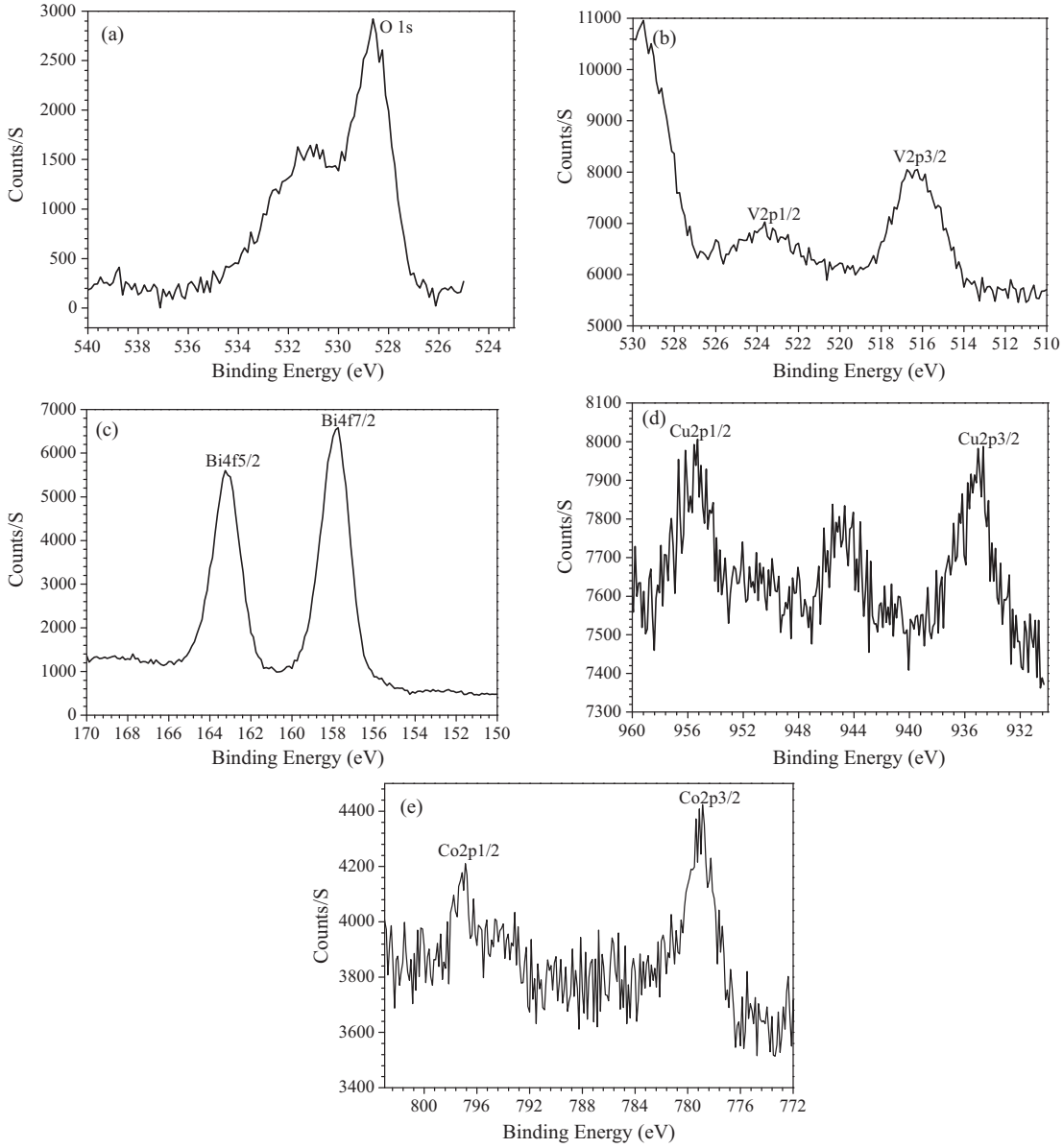

Fig. 3. The high-resolution XPS spectra of the core levels of O 1s (a), V 2p (b), Bi 4f (c), Cu 2p (d) and Co 2p (e).

3.5. PL properties

PL emission spectra are often used to examine the efficiency of charge carrier trapping, immigration and transfer, as well as understand the fate of e^-/h^+ pairs in semiconductor particles. The room temperature PL emission spectra of pure and $BiVO_4$ composites are shown in Fig. 5. Monoclinic $BiVO_4$ has an obvious peak at near 600 nm in the PL spectrum, which is very close to that of tetragonal $BiVO_4$ [38]. The PL peak of this ultrasound fabricated $BiVO_4$ is observed at around 540 nm. About 60 nm blue shift takes place, which may be attributed to small particle sizes of this ultrasound fabricated $BiVO_4$ crystals. The luminescence corresponds to the recombination of the hole formed in the O 2p band and the electron in the V 3d band. The PL peak of the $Co_3O_4/BiVO_4$ nearly disappears. The results clearly show that the recombination of photogenerated charge carrier between O 2p and V 3d is greatly inhibited by the presence of small quantity of Co. Therefore, it can be inferred that the recombination ratio of electron–hole pairs could be reduced and the photocatalytic reaction will be enhanced greatly. As for the $CuO/BiVO_4$, a decrease in PL intensities is also observed. Moreover,

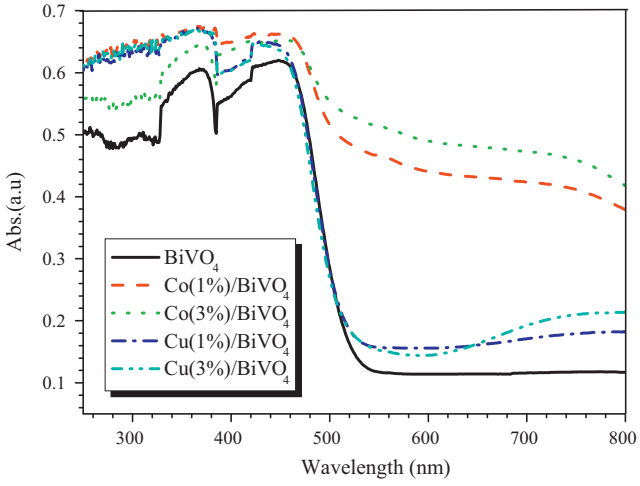

Fig. 4. UV–vis diffuse reflectance spectra of the samples.

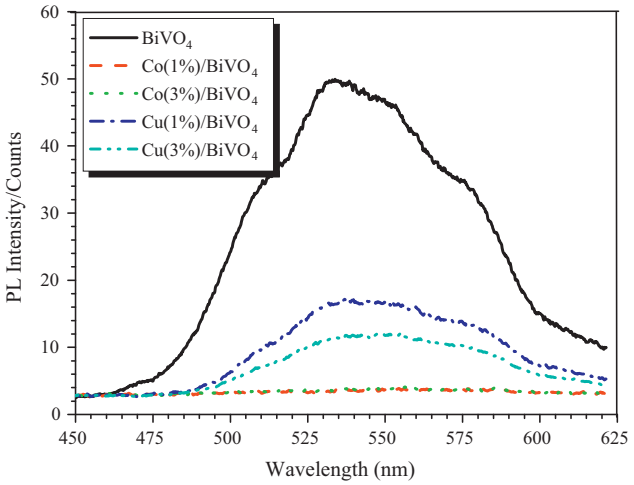

Fig. 5. The photoluminescence (PL) spectra of the samples.

the emission band intensities of the spectra vary with the change of Cu concentration. The high Cu concentration causes a big decrease in the intensity of the PL peak. Therefore, the presence of Cu could also suppress the radiative recombination process, leading to the weak recombination of the e^-/h^+ pairs and high photon efficiency.

3.6. Formation mechanism of the CuO and Co_3O_4/$BiVO_4$ composites under ultrasound irradiation

A series of chemical reactions including hydrolysis, oxidation, reduction, dissolution, and decomposition can be induced by intense ultrasonic irradiation [39,40]. The elevated temperatures and pressures produced by the effects of acoustic cavitation could cause the pyrolysis of water into H• and OH• radicals. The OH• radicals can integrate each other to form H_2O_2. The formation of Co_3O_4 occurs from cobaltous acetate, which could be produced by sonochemical hydrolysis with oxidation. Whereas sonochemical hydrolysis alone could be responsible for the formation of ZnO from its acetate. According to the formation mechanism of $ZnFe_2O_4$ described in literature [40], the following similar reaction steps for the formation of Co_3O_4 and ZnO mediated by ultrasound cavitation were proposed.

$$H_2O \xrightarrow{\text{ultrasound}} H^\bullet + OH^\bullet \quad (1)$$

$$H^\bullet + H^\bullet \rightarrow H_2 \quad (2)$$

$$OH^\bullet + OH^\bullet \rightarrow H_2O_2 \quad (3)$$

$$Co(CH_3COO)_2 + 2H_2O \rightarrow Co(OH)_2 + 2CH_3COOH \quad (4)$$

The produced $Co(OH)_2$ can be oxidized to Co_3O_4 by H_2O_2 generated due to ultrasound cavitation, which is expressed as Eq. (5):

$$Co(OH)_2 + H_2O_2 \rightarrow Co_3O_4 + 4H_2O \quad (5)$$

Sonochemical hydrolysis of copper acetate can result in the formation of ZnO, as shown in the following Eq. (6):

$$Cu(CH_3COO)_2{\cdot}H_2O + H_2O \rightarrow CuO + 2CH_3COOH + H_2O \quad (6)$$

The produced Co_3O_4 and CuO will be uniformly dispersed over $BiVO_4$ by the dispersion role of ultrasound. At the same time, the amorphous $BiVO_4$ can rapidly crystallize to the highly crystalline $BiVO_4$ under this intense ultrasonic irradiation.

3.7. Photocatalytic activity

The photocatalytic activities of the ultrasound fabricated pure and $BiVO_4$ composites were evaluated by measuring the degradation of acid orange II in an aqueous solution under visible light irradiation ($\lambda > 420$ nm). The results are shown in Fig. 6. From Fig. 6(a), it can be seem that acid orange II can only be slightly degraded under visible light irradiation without catalysts, indicating that acid orange II is a stable molecular and the photolysis can be ignored. Compared with pure $BiVO_4$, the composite catalysts show very high photocatalytic activity. Fig. 6(b) gives the degradation rates of the dye over different catalysts after visible light irradiation for 5 h. The values of the degradation rate are 48%, 52%, 86%, 78% and 64% over $BiVO_4$, Co(1%)/$BiVO_4$, Co(3%)/$BiVO_4$, Cu(1%)/$BiVO_4$ and Cu(3%)/$BiVO_4$, respectively. The highest degradation rate is obtained over Co(3%)/$BiVO_4$, which is attributed to the obviously low recombination rate of photogenerated hole–electron pairs due to the presence of Co. However, as for the Cu/$BiVO_4$ catalysts, the high concentration of Cu (3 wt.%) shows the low activity compared with low concentration of Cu (1 wt.%). The reasons for the enhanced photocatalytic activity over the composite photocatalysts are simply suggested as following. Some literatures indicate that CuO [41] and Co_3O_4 [42] are p-type semiconductor and $BiVO_4$ is determined as an n-type material [43]. Therefore, at the interface of the two materials, a p–n hetero-junction would be formed in the composite photocatalysts. The formation of p–n heterojunction with proper energy band positions could effectively restrain the recombination of photogenerated electron–hole pairs [30,31], then enhancing the photocatalysis efficiency.

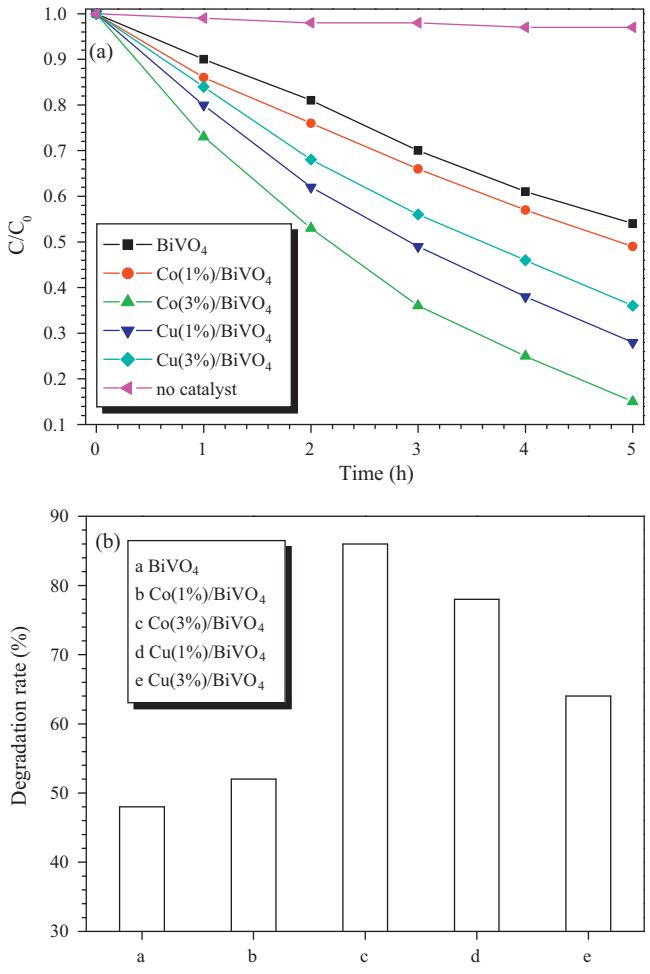

Fig. 6. Decomposition of acid orange II test during irradiation with visible light irradiation: (a) acid orange II concentration changes as a function of irradiation time; (b) degradation rate of acid orange II over different catalysts.

4. Conclusions

Co_3O_4 and $CuO/BiVO_4$ composite photocatalysts were successfully prepared by intense ultrasound irradiation method at room temperature. The fabricated $BiVO_4$ has monoclinic scheelite structures and high crystallinity. The composite photocatalysts exhibit enhanced photocatalytic activity under visible light irradiation. As for $Co_3O_4/BiVO_4$, the highest efficiency is observed at 3 wt.% content and for $CuO/BiVO_4$, 1 wt.% copper content gives the highest photocatalytic activity. The enhanced activity could be attributed to the p–n heterojunction semiconductor structure which effectively restrains the recombination of photogenerated hole–electron pairs.

Acknowledgments

This work was financially supported by the National Natural Science Foundation of China (No. 21067004), Natural Science Foundation of Jiangxi Province (No. 2010GZH0048), the Young Science Foundation of Jiangxi Province Education Office (No. GJJ10150) and Open Foundation of State Key Laboratory of Physical Chemistry of Solid Surfaces, Xiamen University (No. 200906).

References

[1] C.L. Yu, J.C. Yu, M. Chan, J. Solid State Chem. 182 (2009) 1061–1069.
[2] C.L. Yu, J.C. Yu, Catal. Lett. 129 (2009) 462–470.
[3] D.B. Thuan, K. Akira, I. Shigeru, M. Michio, J. Am. Chem. Soc. 132 (2010) 8453–8458.
[4] H.F. Yu, S.T. Yang, J. Alloys Compd. 492 (2010) 695–700.
[5] R.M. Mohamed, I.A. Mkhalid, J. Alloys Compd. 501 (2010) 301–306.
[6] C.L. Yu, J.C. Yu, Mater. Sci. Eng. B 164 (2009) 16–22.
[7] C.L. Yu, D.J. Cai, K. Yang, J.C. Yu, Y. Zhou, C.F. Fan, J. Phys. Chem Solids 71 (2010) 1337–1343.
[8] C. Hu, T.W. Peng, X.X. Hu, Y.L. Nie, X.F. Zhou, J.H. Qu, H. He, J. Am. Chem. Soc. 132 (2010) 857–862.
[9] C.L. Yu, J.C. Yu, Mater. Sci. Eng. B 166 (2010) 213–219.
[10] J.J. Wu, X.J. Lü, L.L. Zhang, Y.J. Xia, F.Q. Huang, F.F. Xu, J. Alloys Compd. 496 (2010) 234–240.
[11] X.G. Han, Q. Kuang, M.S. Jin, Z.X. Xie, L.S. Zheng, J. Am. Chem. Soc. 131 (2009) 3152–3153.
[12] X. Zhang, Z.H. Ai, F.L. Jia, L.Z. Zhang, J. Phys. Chem. C 112 (2008) 747–753.
[13] X.C. Wang, K. Maeda, A. Thomas, K. Takanabe, G. Xin, K. Domen, M. Antonietti, Nat. Mater. 8 (2009) 76–80.
[14] X.L. Huang, J. Lv, Z.S. Li, Z.G. Zou, J. Alloys Compd. 507 (2010) 341–344.
[15] Y.Y. Li, S.S. Yao, W. Wen, L.H. Xue, Y.W. Yan, J. Alloys Compd. 491 (2010) 560–564.
[16] F.Q. Huang, J.J. Wu, X.P. Lin, Z. Zhou, J. Alloys Compd. 509 (2011) 764–768.
[17] L. Ge, J. Mol. Catal. A: Chem. 282 (2008) 62–66.
[18] L. Zhou, W.Z. Wang, L.S. Zhang, J. Phys. Chem. C 111 (2007) 13659–13662.
[19] C.Y. Chung, C.H. Lu, J. Alloys Compd. 502 (2010) L1–L5.
[20] A. Kudo, Int. J. Hydrogen Energy 31 (2006) 197–202.
[21] B.P. Xie, H.X. Zhang, P.X. Cai, R.L. Qiu, Y. Xiong, Chemosphere 63 (2006) 956–963.
[22] H. Xu, H.M. Li, C.D. Wu, J.Y. Chu, Y.S. Yan, H.M. Shu, Mater. Sci. Eng. B147 (2008) 52–56.
[23] S.H. Jung, E. Oh, K.H. Lee, W.J. Park, S.H. Jeong, Adv. Mater. 19 (2007) 749–753.
[24] J.C. Yu, X.C. Wang, L. Wu, W.K. Ho, L.Z. Zhang, G.T. Zhou, Adv. Funct. Mater. 14 (2004) 1178–1183.
[25] Y. Koltypin, S.I. Nikitenko, A. Gedanken, J. Mater. Chem. 12 (2002) 1107–1110.
[26] L. Zhou, W.Z. Wang, S.W. Liu, L.S. Zhang, H.L. Xu, W. Zhu, J. Mol. Catal. A Chem. 252 (2006) 120–124.
[27] W.P. Huang, X.H. Tang, Y.Q. Wang, Y. Koltypin, A. Gedanken, Chem. Commun. (2000) 1415–1416.
[28] J.H. Bang, K.S. Suslick, J. Am. Chem. Soc. 129 (2007) 2242–2243.
[29] S. Tokunaga, H. Kato, A. Kudo, Chem. Mater. 13 (2001) 4624–4628.
[30] H. Xu, H.M. Li, C.D. Wu, J.Y. Chu, Y.S. Yan, H.M. Shu, Z. Gu, J. Hazard. Mater. 153 (2008) 877–884.
[31] M. Long, W. Cai, J. Cai, B. Zhou, X. Chai, Y. Wu, J. Phys. Chem. B110 (2006) 20211–20216.
[32] A. Gulino, I. Fragala, Inorg. Chim. Acta 358 (2005) 4466–4472.
[33] C. Kormann, D.W. Bahnemann, M.R. Hoffmann, J. Phys. Chem. 92 (1988) 5196–5201.
[34] J.G. Yu, J.C. Yu, W.K. Ho, Z.T. Jiang, New J. Chem. 26 (2002) 607–613.
[35] C.S. Cheng, M. Serizawa, H. Sakata, T. Hirayama, Mater. Chem. Phys. 53 (1998) 225–230.
[36] D. Barreca, C. Massignan, S. Daolio, M. Fabrizio, C. Piccirillo, L. Armelao, E. Tondello, Chem. Mater. 13 (2001) 588–593.
[37] F. Li, X. Li, M. Hou, K. Cheah, W. Choy, Appl. Catal. A: Gen. 285 (2005) 181–189.
[38] A. Kudo, K. Omori, H. Kato, J. Am. Chem. Soc. 121 (1999) 11459–11467.
[39] K.S. Suslick, Ultrasound: Its Chemical, Physical and Biological Effects, VCH, Weinheim, Germany, 1988.
[40] S. Manickam, T. Tsuyoshi, I. Hiroshi, T. Atsuya, Y. Kyuichi, T. Toru, K. Teruyuki, B. Dipten, I. Yasuo, J. Phys. Chem. B110 (2006) 15234–15243.
[41] G. Zou, H. Li, D. Zhang, K. Xiong, C. Dong, Y. Qian, J. Phys. Chem. B 110 (2006) 1632–1637.
[42] M. Trari, A. Bouguelia, Y. Bessekhouad, Sol. Energy Mater. Sol. Cells 90 (2006) 190–202.
[43] I.C. Vinke, J. Diepgrond, B.A. Boukamp, K.J. de Vries, A.J. Burggraaf, Solid State Ionics 57 (1992) 83–89.